# Comparison of two fluid codes for modelling 2D instabilities in ExB plasmas

**IEPC-2024-328**

*Presented at the 38th International Electric Propulsion Conference, Toulouse, France*
*June 23-28, 2024*

D. Poli [*], P. Fajardo[†], E. Ahedo[‡]
*Department of Aerospace Engineering, Universidad Carlos III de Madrid, Leganés, Spain*

G. Hagelaar[§]
*LAPLACE, Université de Toulouse, CNRS, INPT, UPS, Toulouse, France*

**Partially magnetised ExB plasmas are used in many devices, from surface processing to space propulsion, allowing for efficient ionisation or ion acceleration. However, these plasmas are subject to many instabilities, leading to a reduction of the magnetic confinement by enhancing the cross-field transport, but the details of this process are not well known. Among the various modelling techniques to analyse that phenomenon, the fluid description offers a more direct interpretation of the physical processes, solving directly for the macroscopic plasma properties. However, the model assumptions can strongly affect the simulated discharge behaviour. This work compares two full-fluid codes, independently developed at the Lapalce laboratory and at the Universidad Carlos III de Madrid, with different treatments of quasi-neutrality and electron inertia. In the proposed test cases, consisting of an isothermal magnetised plasma column and plasma layer, the plasma develops large-scale instabilities: the different modelling assumptions lead to non-negligible discrepancies in the saturated regimes of the instabilities and the resulting cross-field transport.**

[*]PhD student, Equipo de propulsión espacial y plasmas, davide.poli@pa.uc3m.es.
[†]Professor, Equipo de propulsión espacial y plasmas, pfajardo@ing.uc3m.es.
[‡]Professor, Equipo de propulsión espacial y plasmas,eahedo@ing.uc3m.es.
[§]Senior researcher at CNRS, LAPLACE, gerjan.hagelaar@laplace.univ-tlse.fr.

# I. Introduction

Partially magnetized ExB plasmas are commonly found in many devices, from surface processing magnetrons and Penning traps to Hall Effect thrusters (HET). The usage of perpendicular electric and magnetic fields allows the sustainment of plasma discharges via impact ionization even at low densities, or as in the case of HETs, it enables the imposition of strong electric fields that can be used to accelerate ions. However, it is well-known[1] that ExB plasmas exhibit many instabilities, which lead to a reduction of the magnetic confinement and the cross-field transport, generally reducing the device's efficiency. The current understanding of such phenomena is limited, and while the linear stability theory[2] is useful to have a physical insight into the onset of the phenomenon, the use of non-linear simulations is necessary to characterize it. Particle-in-cell (PIC) simulations[3–5] are the most common approach, thanks to the capability of resolving, at affordable computational cost, kinetic effects and non-Maxwellian velocity distribution functions. However, interpreting PIC results can be challenging, especially when trying to isolate the triggering mechanism of certain phenomena, since they describe a vast amount of physics from a microscopic point of view. On the contrary, fluid models deal directly with the macroscopic measurable properties of the plasma. They can predict many instabilities in a wide frequency range at the cost of not being able to resolve kinetic effects and being limited to near Maxwellian VDF.

In the two-fluid (electrons and singly-charged ions) formulation, different assumptions can be made on the level of accuracy of the modelled physics, usually gaining computational speed in the simpler models. A common approximation is the 5-moment model, which can consider non-neutrality and inertial terms, or assume the quasi-neutral (and usually drift-diffusion for electrons) formulation. The second approach usually results in a much shorter computational time, not being constrained in time step and cell sizes by the plasma frequency, electron cyclotron frequency and Debye length. However, in some cases, the model assumptions can strongly affect the results, thus obtaining an unreliable description of the physical problem.

In this preliminary work, two fluid codes, based on the non-neutral fully inertial and the quasi-neutral assumptions, are used to analyse and compare the onset of instabilities in ExB plasmas. Two ExB configurations are investigated, in which isothermal ions and electrons are considered, showing the underlying differences in the modelling strategies, both in modelled physics and numerical methods. The models are described in Sec.II, with the boundary conditions and integration techniques, and the preliminary results are reported in Sec.III.

# II. Model and codes description

This section briefly describes the two full fluid codes used in the comparison. The Universidad Carlos III de Madrid has developed the first code whereas the second one, called MAGNIS[6] has been developed by Gerjan Hagelaar at the Laplace laboratory in Toulouse. Even though the codes present differences in the quasi-neutrality assumption and the solution method, the models formally solve the same equations for ions and electrons (in this work neutrals are never modelled as an evolving fluid). This work uses the isothermal (for both ions and electrons) version of the codes. This choice has been driven by the already complex behaviour of the discharge and the difficulty in comparing the energy equations with different heat-flux closures. The general fluid equations in their conservative form can be written as follows:

$$\frac{\partial n_e}{\partial t} + \nabla \cdot (n_e \mathbf{u}_e) = S_p, \tag{1}$$

$$\frac{\partial n_i}{\partial t} + \nabla \cdot (n_i \mathbf{u}_e) = S_p, \tag{2}$$

$$\frac{\partial (n_e \mathbf{u}_e)}{\partial t} + \nabla \cdot (n_e \mathbf{u}_e \mathbf{u}_e) = -\frac{1}{m_e}\nabla p_e + \frac{e n_e}{m_e}(\nabla\phi - \mathbf{u}_e \times \mathbf{B}) - n_e \nu_e^m \mathbf{u}_e, \tag{3}$$

$$\frac{\partial (n_i \mathbf{u}_i)}{\partial t} + \nabla \cdot (n_i \mathbf{u}_i \mathbf{u}_i) = -\frac{1}{m_i}\nabla p_i - \frac{e n_i}{m_i}(\nabla\phi - \mathbf{u}_i \times \mathbf{B}), \tag{4}$$

where the isotropic scalar pressure $p_\alpha$ is assumed for each species $\alpha = e, i$, $S_p$ is the plasma production source term, and $\nu_e^m = n_n k_e^m(T_e)$ is the total momentum transfer collision frequency. The rate coefficient $k_e^m(T_e)$ is interpolated from look-up tables pre-calculated with the BOLSIG+[7] software from the cross-section data in the SIGLO[8] database for a Maxwellian electron energy distribution function. With the selected parameters

for the analysed cases, the plasma can be considered weakly collisional. The model considers only the perpendicular component of the magnetic field $\mathbf{B} = B\hat{z}$. The main differences between the codes lay in the quasi-neutrality assumption, the treatment of the electron inertia and the solution algorithm, as detailed below.

### A. 2D Non-neutral code

The non-neutral code (NNC) solves directly for the equations 1-4 in their conservative form, without further manipulation. To account for non-neutral effects, the electrostatic potential is obtained by the solution of the Poisson equation

$$\nabla^2\phi = \frac{e}{\epsilon_0}\left(n_e - n_i\right), \tag{5}$$

discretized with a 5-point stencil finite difference scheme and solved at each timestep with the MUMPS[9] direct solver.

The system of equations is advanced in time with a finite volume method (FVM) algorithm. The electron and ion systems are treated separately but coupled through the Poisson equation. To satisfy the stability criterion of the Euler-Poisson system,[10] the equations cannot be trivially advanced in time explicitly, being the system unconditionally unstable. To overcome this issue, a fractional step method is used to advance separately the homogeneous and the source part of the balance laws. In particular, the second-order accurate Strang splitting scheme is used, computing the new potential between the convective and source term step. The advancing algorithm for a time increment $\Delta t$ is the following:

1. The collision frequencies are interpolated.
2. The source terms are advanced of $0.5\Delta t$.
3. The homogenous system is advanced of $\Delta t$.
4. The Poisson equation is solved with the new densities.
5. The source terms are advanced of $0.5\Delta t$.

The algorithm uses an adaptive time-step, meaning that in every iteration the time-step is computed to satisfy the CFL constraint and to resolve the plasma frequency.

For what concerns the hyperbolic homogeneous system, a Riemann solver based approach is used. The available Riemann solvers are Rusanov, Roe, HLL, HLLE and HLLC, to be coupled with a MUSCL 2nd order reconstruction scheme with *minmod* slope limiter. The HLLC[11] solver is used in all the simulations presented in this work, with the addition of a low-Mach correction.[12] The source terms and the homogenous systems are advanced in time using a third-order strong stability preserving Runge-Kutta scheme.[13] The algorithm is written in FORTRAN and parallelized with MPI domain decomposition.

Boundary conditions A variety of boundary conditions can be set for the different fluid species, but for the analysis performed in this work only the periodic and sheath boundary conditions will be used. Periodic boundary conditions assume the usual formulation and thus are not discussed further; for what concerns sheath boundary conditions, the approach introduced by Sahu et al.[14] has been used. In such formulation, the drifted Maxwellian velocity distribution function is integrated to recover the mass and momentum in the two directions, respectively:

$$\Gamma_{1\alpha} = \pm n_\alpha \frac{\bar{c}_\alpha}{4}\left[\exp(-\tilde{u}_{\perp\alpha}^2) + \sqrt{\pi}\tilde{u}_{\perp\alpha}\big(\mathrm{erf}\ \tilde{u}_{\perp\alpha} \pm 1\big)\right], \tag{6}$$

$$\Gamma_{2\alpha} = \pm n_\alpha T_\alpha \left[\frac{\tilde{u}_{\perp\alpha}}{\sqrt{\pi}}\exp(-\tilde{u}_{\perp\alpha}^2) + \left(\frac{1}{2} + \tilde{u}_{\perp\alpha}^2\right)\big(\mathrm{erf}\ \tilde{u}_{\perp\alpha} \pm 1\big)\right], \tag{7}$$

$$\Gamma_{3\alpha} = m_\alpha u_{\parallel\alpha}\Gamma_{1\alpha}, \tag{8}$$

where $u_\perp, u_\parallel$ are the perpendicular and parallel velocities to the wall, $\tilde{u}_{\perp\alpha} = u_{\perp\alpha}(2T_\alpha/m_\alpha)^{-0.5}$ is the normalised velocity, and $\bar{c}_\alpha = (8T_\alpha/\pi m_\alpha)^{0.5}$ the thermal speed; the $\pm$ depends on the direction of the cell face normal. At each iteration of the algorithm, the boundary fluxes are imposed directly in the finite volume scheme. Dirichlet conditions are used for the Poisson equation.

## B. MAGNIS

Contrary to the NNC, MAGNIS assumes quasi-neutrality ($n_e \approx n_i$) and thus the Poisson equation is not used, removing the constraint of the Debye length. The electrostatic potential is computed from the momentum and the current conservation equation

$$\nabla \cdot (n_i \mathbf{u}_i - n_e \mathbf{u}_e) = 0, \tag{9}$$

yielding a second-order equation in $\phi$. As opposed to the NNC, in MAGNIS, the fluid equations are expressed in their non-conservative form, which for the momentum equations of ions and electrons read:

$$\frac{\partial \mathbf{u}_i}{\partial t} + \mathbf{u}_i \cdot \nabla \mathbf{u}_i = -\frac{e}{m_i} (\nabla \phi - \mathbf{u}_i \times \mathbf{B}) - \frac{\nabla p_i}{m_i n_i} - \frac{S_p}{n_i} \mathbf{u}_i, \tag{10}$$

$$0 = \frac{e}{m_e} (\nabla \phi - \mathbf{u}_e \times \mathbf{B}) - \frac{\nabla p_e}{m_e n_e} - \left( \nu_e + \frac{S_p}{n_e} \right) \mathbf{u}_e - \beta \frac{\partial \mathbf{u}_e}{\partial t}, \tag{11}$$

where $\beta = \max(1, \omega_c \Delta t)$ is a relaxation factor to ensure numerical stability even in the case of a large Hall parameter, known to be a problem for quasi-neutral codes. As it can be seen, the electron inertia is not properly resolved, and even though the temporal term is retained as a source term, the model must be intended as a drift-diffusion approximation of electrons.

As for the NNC, the equations are advanced in time using a FVM with 2nd-order MUSCL reconstruction; however, contrary to the NNC, MAGNIS uses a predictor-corrector scheme in a segregated algorithm to update the fluid variables, employing both explicit and implicit time-stepping algorithms. The integration algorithm of MAGNIS is summarised as follows (a more detailed description is reported in the thesis of Sadouni[6]):

1. Collision frequencies, sources and wall speeds for boundary conditions are calculated.
2. Electron and ion velocities are predicted from the momentum equations including the inertia term.
3. The electric field and potential are solved from the current conservation equation, accounting for the response of the particle velocities to change in $-\nabla\phi$ to satisfy the current continuity.
4. The particle velocities are corrected with the new electric field (here $\frac{\partial \mathbf{u}_e}{\partial t}$ is not considered).
5. Ion density $n_i$ is solved using the new velocities.
6. The electron density $n_e$ is updated with the quasi-neutral assumption.

The algorithm is repeated until the end of the simulation with a fixed time-step: the partial introduction of electron inertia with the semi-implicit schemes poses no constraints on the time step other than the CFL condition. The code is implemented in FORTRAN and no parallelization is used.

Boundary conditions The boundary conditions in MAGNIS are imposed at the boundary with lateral walls (either conductive or dielectric) unless a periodic domain is used. Because of the quasi-neutrality assumption, the boundary conditions are specified at the sheath edge according to the classical sheath model. The boundary condition for the particle flux is expressed as:

$$(n_\alpha u_{\perp \alpha}) = \pm n_\alpha W_\alpha, \tag{12}$$

where $W$ is an effective wall loss speed computed from the classical sheath theory accounting for the direction of the cell face normal. For electrons and ions:

$$W_e = \left( \frac{T_e}{2\pi m_e} \right)^{1/2} \exp\left( -\frac{e(\phi - \phi_w)}{T_e} \right), \tag{13}$$

$$W_i = \max\left[ \left( \frac{T_e}{m_i} \right)^{1/2}, |u_{\perp i}| \right], \tag{14}$$

where $\phi$ is the potential at the sheath edge computed by the code and $\phi_w$ is the imposed potential at the wall; Eq.(14) is the Bohm condition. Dirichlet boundary conditions are used for the potential at the wall.

# III. Results

In the following subsections, two test cases of ExB plasmas are presented, consisting of a magnetised plasma column and a simplified variation in which one direction assumes periodic boundary conditions. The simulations have been performed with the NNC and MAGNIS using the same input parameters, except for time-step and the simulation time. Typically, the simulation time is of 100 µs, however, MAGNIS appears to be slower in reaching the steady state condition on the mean plasma density in the domain, especially in the semiperiodic cases, which have then been run for 200 µs. For all the simulations, molecular hydrogen has been used.

## A. Isothermal magnetised plasma column

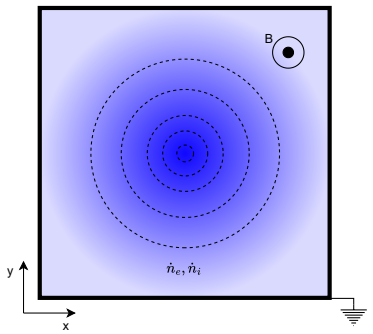


**Figure 1. Schematic of the isothermal magnetised plasma column simulation in a square domain of size L. Electrons and ions are injected with a Gaussian profile.**

The first test case analysed consists of a simplified model of a magnetised plasma column, where the plasma is assumed to be isothermal. The setup is shown in Fig. (1), and must be intended as a section of a plasma column where the out-of-plane dynamics is neglected, the magnetic field is perpendicular to the domain and the lateral walls are grounded. The discharge is sustained by a constant injection of ions and electrons following a Gaussian distribution; the production source term can be thus expressed as:

$$S_p = \frac{I}{e}\frac{f(x,y)}{\int_A f(x,y)dA}, \qquad f(x,y) = \exp\left(-\frac{(x-x_0)^2}{2\ell^2} - \frac{(y-y_0)^2}{2\ell^2}\right) \tag{15}$$

where $I$ [A/m] is a given current, $A$ the computational domain's surface and $x_0, y_0, \ell$ the parameters defining the Gaussian profile. The simulation is initialised with uniform density and $n_e = n_i$. The main simulation parameters are reported in Tab.1.

Unmagnetised case In the unmagnetised case, the plasma column converges to the usual diffusion profile, reaching a steady state condition where for the electrons, the electrostatic force balances the pressure gradient. In this condition, the two codes show good agreement, as shown in Fig.2, except for the lateral sheaths and a higher potential for the NNC. The higher potential is possibly due to numerical inaccuracies in the resolution of the electron momentum inside the sheath due to excessive numerical diffusion. Even though a possible fix has been proposed by Reboul et al.[15] for a simple 1D sheath, the complexity of the 2D case with the addition of magnetised and turbulent plasma has not been explored yet. Since the electric field shows perfect agreement (outside the sheath region), the shift in the potential has been ignored, not seeming to affect the onset of the instabilities. The potential discrepancies will be addressed in future works.

**Table 1. Nominal parameters for the magnetised plasma column test case.**

| Parameter | Value |
|---|---|
| $L$ | 10 cm |
| Cell x | 512 |
| Cell y | 512 |
| $I$ | 50 mA |
| $n_{e0}$ | $10^{14}$m$^{-3}$ |
| $n_{i0}$ | $10^{14}$m$^{-3}$ |
| $n_{n0}$ | $10^{20}$m$^{-3}$ |
| $T_e$ | 2 eV |
| $T_i$ | 0.01 eV |
| $\ell$ | 1 cm |

Onset of the instability It is known[16,17] that in the magnetised plasma column a large-scale instability develops to untrap the magnetised electrons from their gyromotion and facilitate the cross-field transport in the radial direction. In this case, the instability is not linked to the ionisation terms, as it has been observed in magnetron discharges,[18] being the production source term constant and not dependent on the local plasma density.

The instability can be triggered by increasing the magnetic field to the point where the usual diffusion profile is destabilised, as shown in Fig. 3. The plasma column develops large arm-like structures, which at lower magnetic fields are stationary (e.g. at B=11G). Magnetic confinement increases for larger magnetic

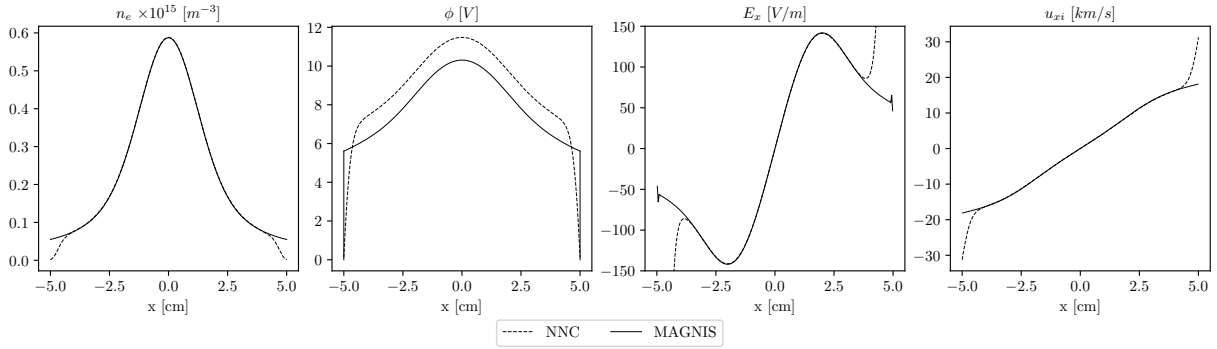


**Figure 2. Steady state solution of the non-magnetised plasma column for MAGNIS and the NNC for the parameters in Tab.1.**

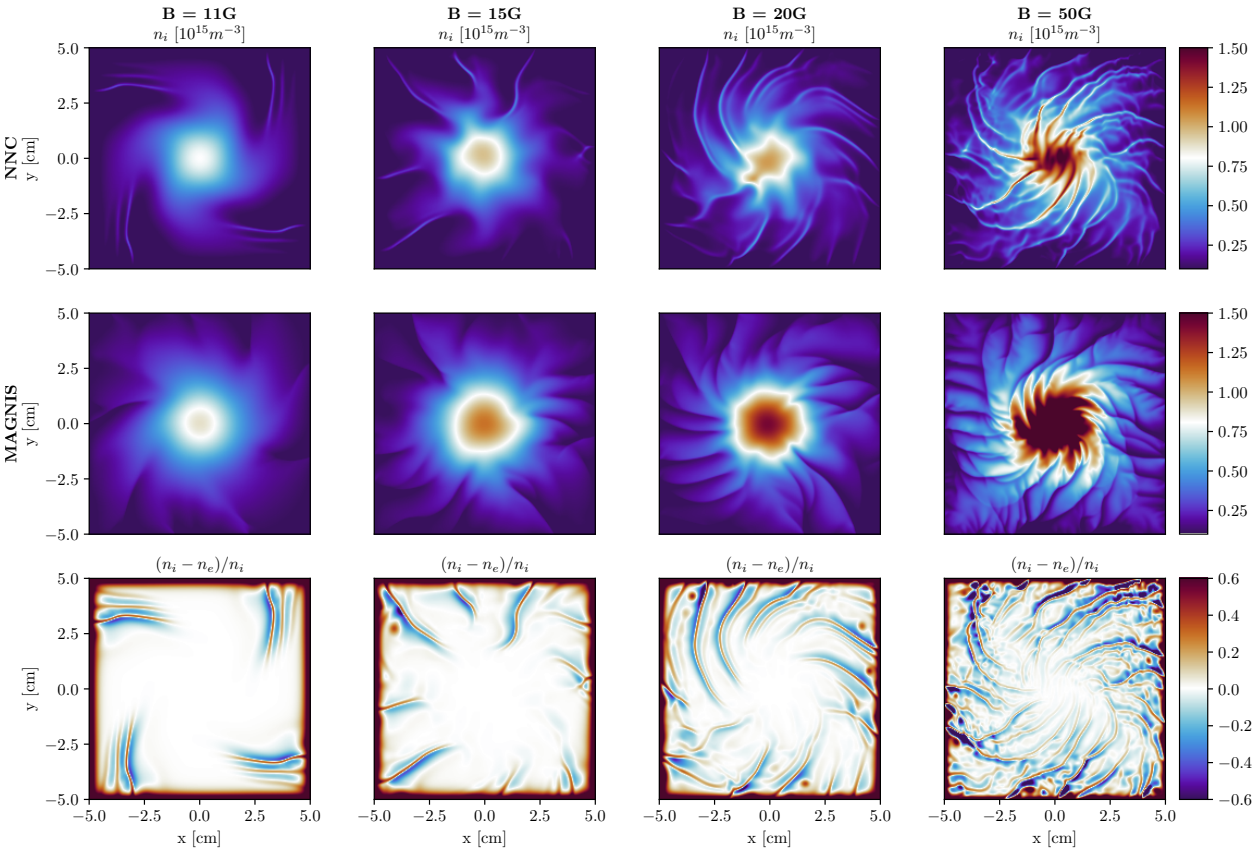


**Figure 3. Istantaneous electron density at different magnetic fields for the NNC (top) and MAGNIS (middle), and charge density for the NNC (bottom).**

fields, resulting in a larger peak plasma density for the same $I$. In turn, the plasma column develops a stronger instability to transport plasma to the wall, characterised by the formation of finer structures rotating in the diamagnetic drift direction (corresponding to $-\mathbf{E} \times \mathbf{B}$ in this case). The diamagnetic drift dominates the electron motion, while the weakly magnetised ions have a predominantly radial velocity.

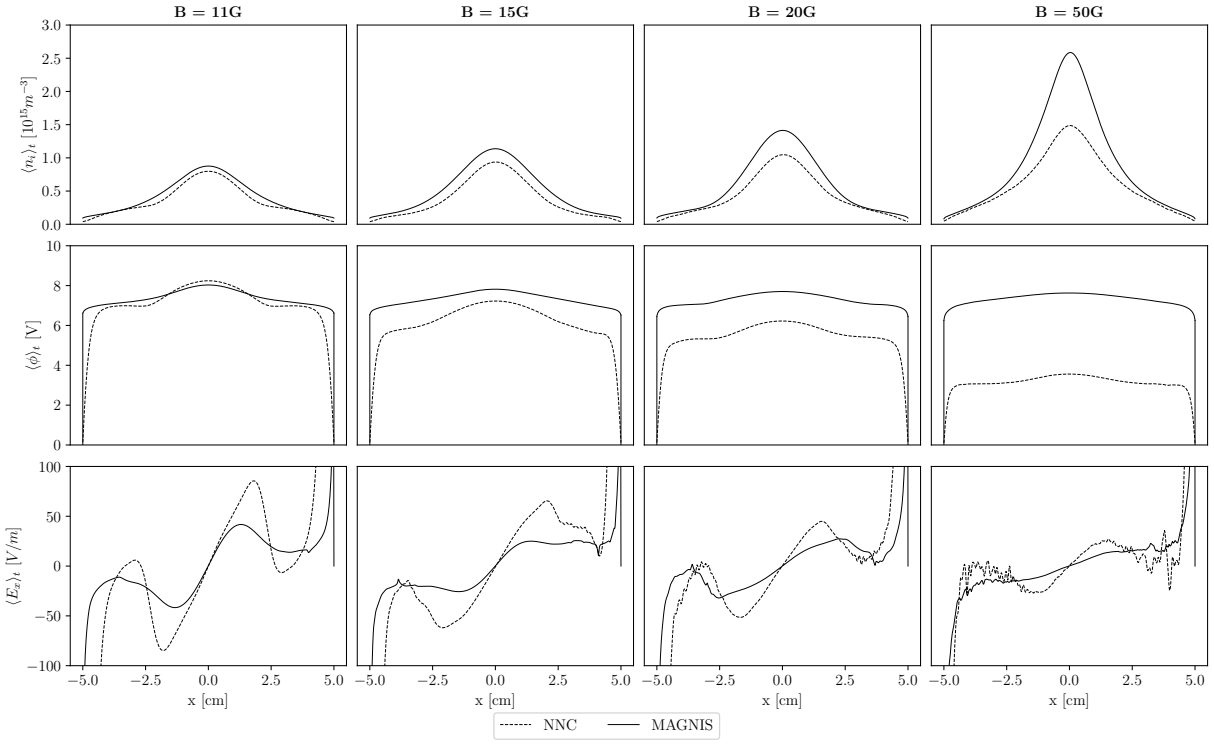


**Figure 4. Time averaged profiles of the plasma density (top) and potential (middle) and electric field (bottom) at $y$ =5 cm.**

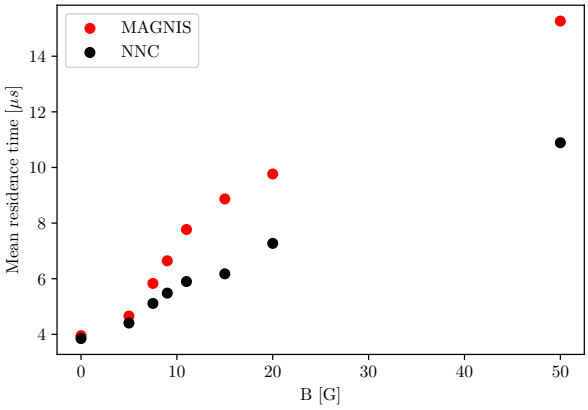


**Figure 5. Mean residence time of the magnetised plasma column at different B for MAGNIS and the NNC.**

This behaviour is consistent between the two codes, even though in the NNC the filament structures are more accentuated, as shown in Fig.3. In the NNC, these structures are associated with non-negligible charge separation (shown in the last row of Fig.3), which is consistent with PIC simulations of rotating spokes[19] where a double layer is formed at the edge of the spoke. As the magnetic field increases, the plasma becomes more turbulent and the charge separation becomes more important. Although MAGNIS can capture sharp gradients in the electric field, it cannot resolve charge separation on a finite scale due to the hypothesis of quasi-neutrality, coincident with $\epsilon_0, \lambda_d \to 0$, thus some differences are to be expected.

The mean profiles of $n_i, \phi, E_x$ averaged over 30 µs are shown in Fig. 4. At larger magnetic fields the difference in the predicted plasma density becomes more important, highlighting the increased cross-field transport present in the NNC model. Common to the two codes is predicting a smaller electric field as the magnetic field increases, as shown in the last row of Fig.4. This is consistent with the larger magnetic force balancing the pressure gradient in the electron momentum equation, thus a smaller electric field is needed. Once again it can be observed how the instability of the NNC reduces the magnetic confinement, leading to larger values of $E_x$ than in MAGNIS. The differences in the sheath potential can be attributed to similar effects, noticing that electrons become progressively

magnetised in the sheath region.

A way to approximately quantify the turbulent transport is to define a mean residence time[6] as:

$$\tau = \frac{\langle \int_V n_i dV \rangle_t}{\langle \int_V S_p dV \rangle_t}, \tag{16}$$

corresponding to the ratio of the average plasma density over the average ionisation source $S_p$; the averaging is done over 50 µs. In other words, $\tau$ represents how fast the injected plasma reaches the lateral walls. According to this definition, the mean residence time increases as the magnetic confinement becomes more efficient in trapping the electrons; thus $\tau$ is expected to grow at larger magnetic fields. This behaviour can be observed in Fig.5 where the mean residence time is shown for the NNC and MAGNIS at different magnetic fields. The small difference in $\tau$ at $B = 0$ is due to lateral sheaths in the NNC, which inevitably results in a lower average ion density in the domain with the same source term. However, it can be observed how the NNC predicts a slower increase of the mean residence time, especially in correspondence with the onset of the finer filament structures at $B \approx 10$G, indicating a faster transport of plasma across the magnetic field. Even though the mean residence time is not a direct measurement of the turbulent cross-field transport, it is helpful to the general behaviours of the codes, showing non-negligible differences in the efficiency of the magnetic confinement.

## B. Isothermal semi-periodic plasma layer

The second test case consists of a semi-periodic (along the y direction) domain with lateral grounded walls. As in the previous case, ions and electrons are injected at the centre of the domain following a Gaussian profile along $x$ and uniform along the periodic direction following:

$$\begin{aligned} S_p &= \frac{I}{e} \frac{f(x)}{\int_A f(x) dA}, \\ f(x) &= \exp\left( -\frac{(x - x_0)^2}{2\ell^2} \right). \end{aligned} \tag{17}$$

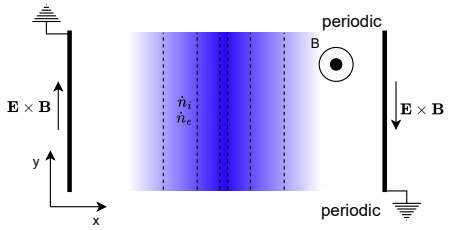


**Figure 6. Schematic of the semi-periodic test case. Ions and electrons are injected with a constant Gaussian profile on the $x$ coordinate.**

The parameters of the Gaussian and the injected current $I$ have been kept identical to the previous test case. The simulation is again initialised with uniform density and $n_e = n_i$; the species temperatures and the magnetic field are uniform and constant. The simulation setup is shown in Fig.6 and the parameters are reported in Tab.2, where only the changes with respect to Tab.1 are shown.

**Table 2. Nominal parameters for the isothermal plasma layer case.**

| Parameter | Value |
|---|---|
| $L_x$ | 10 cm |
| $L_y$ | 5 cm |
| Cell x | 512 |
| Cell y | 256 |

As for the magnetised plasma column, the first comparison between the codes has been performed with $B = 0$. The axial profiles at steady state are reported in Fig.7, where again the codes show very good agreement in the plasma density, ion velocity and electric field. The plasma properties are constant in the $y$ direction. As in the previous test case, the potential in the NNC is larger than in MAGNIS. In this regard, the same considerations for the magnetised plasma column also apply in this scenario.

ONSET OF THE INSTABILITY Similarly to the previous case, by increasing the magnetic field, the magnetised electrons are trapped in a drift motion along the periodic direction $y$. Due to the simulation geometry, the domain can be divided into two antisymmetric regions in the axial direction, where the electrons drift in opposite directions. The plasma confinement is once again reduced by the onset of an instability developing in the periodic direction which limits the maximum plasma density in the domain once the saturation regime is reached. In the NNC the steady state condition of the average plasma density is reached under 100 µs, whereas MAGNIS requires almost twice as much, converging at a much larger density due to the reduced cross-field transport and better confinement. The onset of the instability itself happens much earlier in the simulation of the NNC than in MAGNIS. The electron density and the electric field along $y$ in the saturated regime of the instability with $B = 50$G are shown in Fig.8 for the two codes.

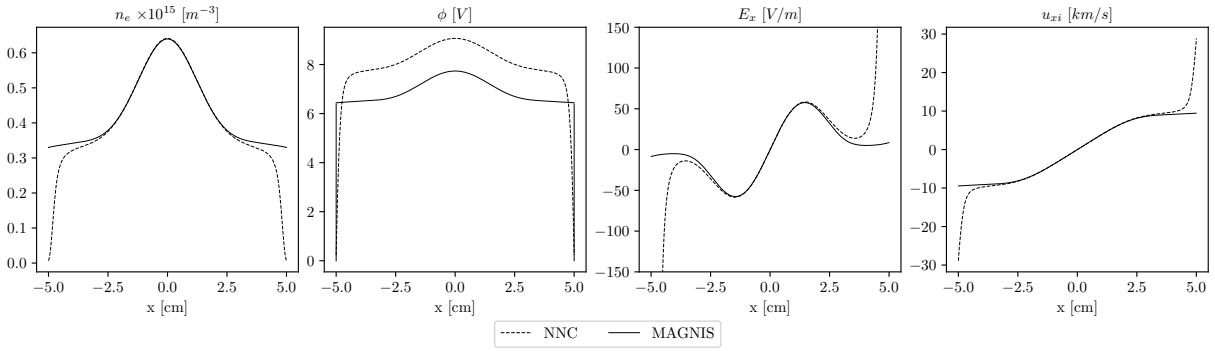


**Figure 7. Steady state solution of the unmagnetised semi-periodic test case for MAGNIS and the NNC for the parameters in Tab.2.**

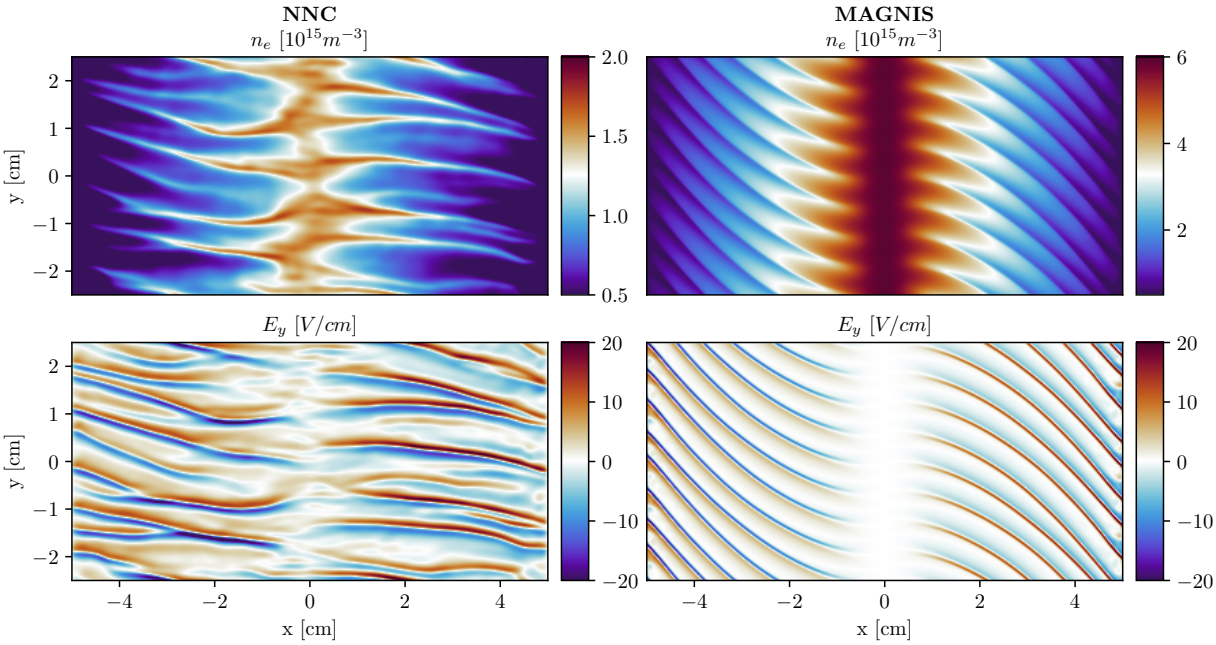


**Figure 8. Electron density (top) and $E_y$ (bottom) for the isothermal plasma layer test case at 50G.**

The instability is characterised by the formation of thin spokes travelling in the $-\mathbf{E} \times \mathbf{B}$ direction with a velocity close to the ion sound-speed $c_s = [(T_e + T_i)/m_i]^{0.5}$. The antisymmetry of the initial condition is preserved and the spokes travel in opposite directions in the two half-domains.

Contrary to Fig.3, where the saturated regimes in the two codes were similar, the models converge to sensibly different solutions. MAGNIS predicts extremely regular structures of $n_e$ and $E_y$, whereas the NNC shows finer and more irregular distribution of the plasma density and electric field. The finer, filament-like structures predicted by the NNC are in line with the results shown in Fig.3, although in this case the difference is more accentuated. Even though the instability predicted by the two models seems to be substantially different, the frequency appears to be in the same order of magnitude. The FFT of the density oscillations sampled by a virtual probe at $x = 0.5cm, y = 2.5cm$ is shown in Fig.9. As in the previous case, the more turbulent instability of the NNC appears to be more efficient in enhancing the cross-field transport, as can be inferred by observing the much higher plasma density in MAGNIS.

Finally, it is interesting to note that the region where the electron drift velocity changes sign (i.e. the antisymmetry plane of the simulation) is subject to very different behaviour. In MAGNIS, the interface between the opposite streaming flows is perfectly preserved, as can be deduced by the uniform density and $E_y = 0$ shown in Fig.8, whereas in the NNC it is quickly destabilised and a mixing of the two regions can be observed. At the current state of the analysis, it is not straightforward to explain the reason for the more stable discharge observed in MAGNIS, which can be due to numerical or physical considerations. It must be kept in mind that MAGNIS lacks the resolution of Poisson and electron inertia, which can play a role in the more turbulent behaviour of the NNC.

NUMERICAL DIFFUSION To evaluate whether the observed differences are numerical or physical, it is necessary to address the problem of numerical diffusion. Fluid codes are inevitably subject to a certain amount of numerical diffusion introduced by the numerical algorithm used to solve the equations. The term numerical diffusion is very broad and thus it is difficult to quantify it precisely. In general, the effect of too large numerical diffusion is the loss of details in the solution, where the sharp features are smeared; this can have a dramatic effect on the prediction of the instabilities. For instance, in the case of cross-field transport, a large numerical diffusion can contribute to the diffusion of plasma across the magnetic field, thus completely inhibiting the formation of the instability itself. The effect of increasing the numerical diffusion can be observed in Fig.10. In the case of the NNC (left), the numerical diffusion can be increased by selecting a different Riemann solver (from HLLC to Rusanov, which is much more diffusive) and removing the 2nd-order MUSCL reconstruction. As expected, the fine structures of the instability are lost and density distribution appears to be much more regular. In MAGNIS, the main way to introduce numerical diffusion is by reducing the number of cells. The usage of a coarser grid does not appreciably alter the already very regular instability, except for predicting a lower frequency. However, this can be attributed to the lack of proper modelling of electron inertia in MAGNIS, thus failing to reach mesh convergence and thus predicting finer structures as the cell size is reduced.

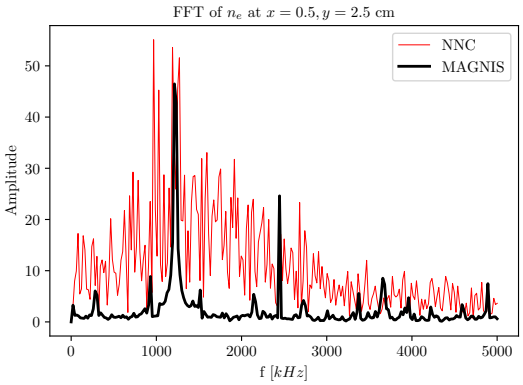


**Figure 9. Fast Fourier transform of $n_e$ sampled at the virtual probe ($x = 0.5cm, y = 2.5cm$) for MAGNIS and NNC.**

Even though this simple comparison is not enough to rule out the influence of numerical diffusion, it appears that, even in the most diffusive configuration, the NNC does not recover the instability predicted by MAGNIS. More detailed analyses on the matter are left for future works.

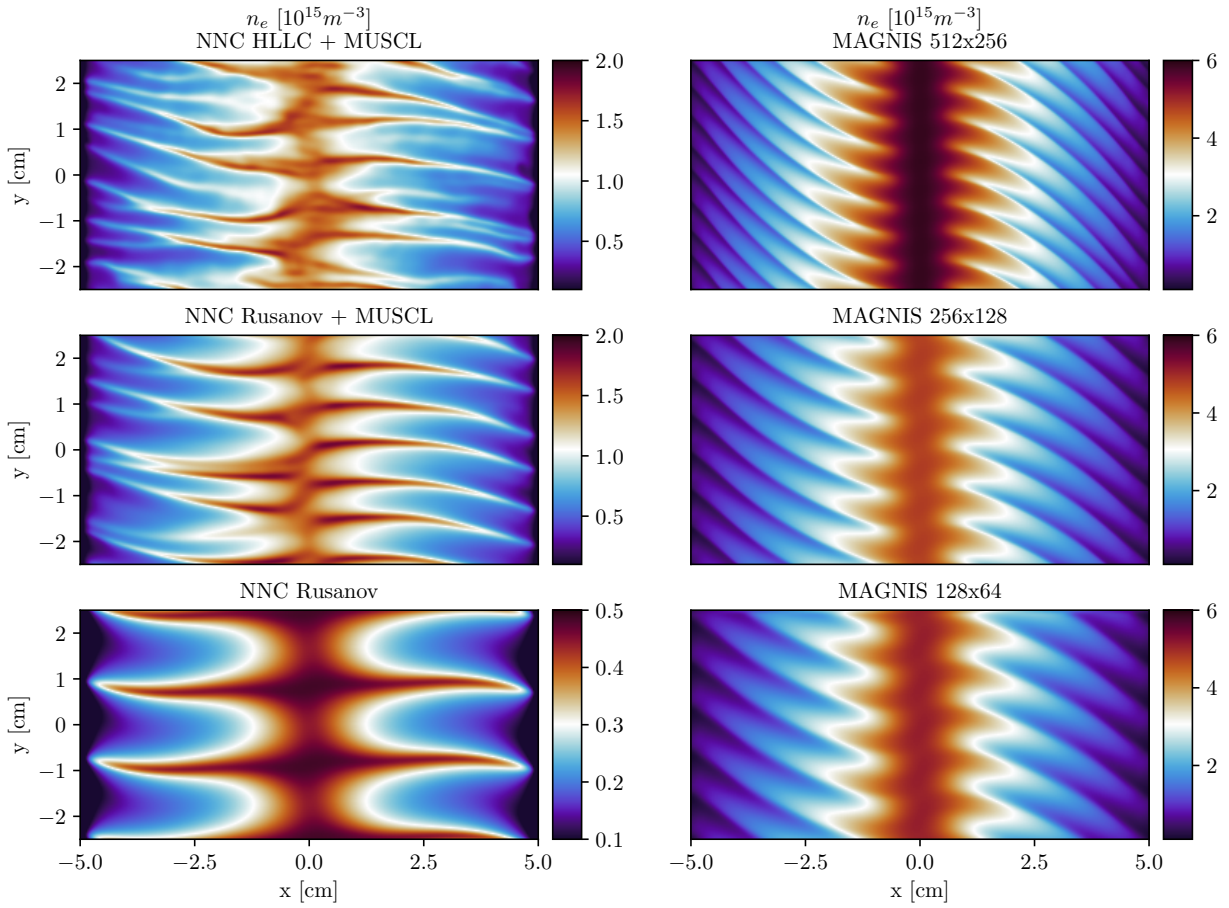


**Figure 10. Effects of numerical diffusion on the NNC (left) and MAGNIS (right) solutions of the semi-periodic test case at 50G. Note the change of scale for the most diffusive solution of the NNC.**

## IV. Conclusions

In this work, two full fluid models of ExB plasma discharges are analysed. The NNC assumes the two-fluid plasma model including electron inertia and accounting for non-neutrality. The system of equations is advanced in time with a Strang-Splitting method, using Runge-Kutta for the time integration and the HLLC approximate Riemann solver with MUSCL reconstruction for the spatial discretisation. The MAGNIS code instead, is a quasi-neutral model with partial inclusion of the electron inertia. Analogously to the NNC, MAGNIS uses a finite volume method discretisation with MUSCL reconstruction, although the equations are integrated with a predictor-corrector scheme.

The codes have been compared by simulating a magnetised plasma column and a semi-periodic variant with grounded lateral walls. Both test cases assume fixed virtual ionisation and isothermal species; the constant magnetic field is perpendicular to the domain and spatially uniform. Different magnetic field intensities have been considered. The simulations have been run until the average plasma density in the domain reaches the steady state condition.

For both test cases, the models show good agreement in the unmagnetised scenario, reaching the same steady-state solution, except for the lateral plasma sheaths and the potential. The NNC overestimates the potential drop in the sheaths, most likely due to excessive numerical diffusion in the electron momentum equation, although further analysis is necessary. Nonetheless, the predicted electric field in the bulk matches very well.

When the magnetic field is increased, both codes predict the onset of large instabilities that enhance the cross-field transport. In both cases, the NNC predicts the formation of finer and more turbulent structures, resulting in a more efficient plasma transport to the wall than in MAGNIS. This can be assessed by observing the mean residence time in the magnetised plasma column, and the larger peak plasma density at steady state predicted by MAGNIS in all the analysed cases.

Overall, concerning the magnetised plasma column, the two codes develop very similar rotating structures, whereas they show very different behaviours for the semi-periodic domain. In particular, MAGNIS predicts the onset of a very regular instability, responsible of a much smaller cross-field transport than the NNC, for which the turbulent behaviour observed in the plasma column is recovered. In addition, MAGNIS preserves the antisymmetry of the simulation step, whereas the NNC predicts a mixing of the counter-streaming flows of plasma. To investigate whether the differences can be due to an excessive numerical diffusion, a preliminary analysis has been performed by analysing progressively more diffusive simulations. However, it appears that even though numerical diffusion plays an important role in the prediction of the instability, it is not the cause of the discrepancies between the two codes. More analysis on the subject is left for future works.

## Acknowledgments

This work has been supported by the R&D project HEEP (PID2022-140035OB-I00) funded by MCIN/AEI/10.13039/501100011033 and by "ERDF A way of making Europe". D. Poli thanks the GREPHE team in LAPLACE laboratory of CNRS Toulouse for the opportunity to carry out the research activity in their premises, as part of the research stay in his PhD thesis.

## References

[1]Jean-Pierre Boeuf and Andrei Smolyakov. Physics and instabilities of low-temperature E x B plasmas for spacecraft propulsion and other applications. *Physics of Plasmas*, 30(5), 2023.

[2]J. J. Ramos, E. Bello-Benítez, and E. Ahedo. Local analysis of electrostatic modes in a two-fluid E x B plasma. *Physics of Plasmas*, 28(5):052115, 2021.

[3]Johan Carlsson, Igor Kaganovich, Andrew Powis, Yevgeny Raitses, Ivan Romadanov, and Andrei Smolyakov. Particle-in-cell simulations of anomalous transport in a Penning discharge. *Physics of Plasmas*, 25(6), 2018.

[4]A.T. Powis, J.A. Carlsson, I.D. Kaganovich, Y. Raitses, and A. Smolyakov. Scaling of spoke rotation frequency within a penning discharge. *Physics of Plasmas*, 25(7):072110, 2018.

[5]W Villafana, G Fubiani, L Garrigues, G Vigot, B Cuenot, and O Vermorel. 3d particle-in-cell modeling of anomalous electron transport driven by the electron drift instability in hall thrusters. In *37th International Electric Propulsion Conference (IEPC-2022)*, 2022.

[6]Sarah Sadouni. *Fluid modeling of transport and instabilities in magnetized low-temperature plasma sources*. Phd thesis, Université Paul Sabatier - Toulouse III, February 2020.

[7]G.J.M. Hagelaar and L.C. Pitchford. Solving the boltzmann equation to obtain electron transport coefficients and rate coefficients for fluid models. *Plasma Sources Science and Technology*, 14:722, 2005.

[8]Siglo database. http://www.lxcat.net. Accessed: June 2013.

[9]P.R. Amestoy, A. Buttari, J.-Y. L'Excellent, and T. Mary. Performance and Scalability of the Block Low-Rank Multifrontal Factorization on Multicore Architectures. *ACM Transactions on Mathematical Software*, 45:2:1–2:26, 2019.

[10]Sylvie Fabre. Stability analysis of the euler-poisson equations. *Journal of Computational Physics*, 101(2):445–451, 1992.

[11]Eleuterio Toro. The hllc riemann solver. *Shock Waves*, 29, 11 2019.

[12]Nico Fleischmann, Stefan Adami, and Nikolaus A. Adams. A shock-stable modification of the hllc riemann solver with reduced numerical dissipation. *Journal of Computational Physics*, 423:109762, 2020.

[13]Sigal Gottlieb and Chi-Wang Shu. Total variation diminishing runge-kutta schemes. *Mathematics of Computation*, 67:73–85, 08 1996.

[14]R. Sahu, A.R. Mansour, and K. Hara. Full fluid moment model for low temperature magnetized plasmas. *Physics of Plasmas*, 27(11):113505, 2020.

[15]Louis Reboul, Marc Massot, and Alejandro Alvarez Laguna. Numerical challenges in the simulation of 1D bounded low-temperature plasmas with charge separation in various collisional regimes. *AIP Conference Proceedings*, 2996(1):190004, 02 2024.

[16]R. Lucken, A. Bourdon, M. A. Lieberman, and P. Chabert. Instability-enhanced transport in low temperature magnetized plasma. *Physics of Plasmas*, 26(7):070702, 07 2019.

[17]A R Mansour and K Hara. Full fluid moment modeling of rotating spokes in penning-type configuration. *Plasma Sources Science and Technology*, 31(5):055012, may 2022.

[18]J. P. Boeuf. Spoke formation in low temperature E x B plasmas: Transition from gradient-drift instability to ionization wave. *Physics of Plasmas*, 30(2):022112, 02 2023.

[19]Jean-Pierre Boeuf and Masayuki Takahashi. Rotating spokes, ionization instability, and electron vortices in partially magnetized E x B plasmas. *Physical review letters*, 124(18):185005, 2020.